INTERNATIONAL JOURNAL FOR NUMERICAL METHODS IN ENGINEERING
Int. J. Numer. Meth. Engng 2003; **56**:1979–1997 (DOI: 10.1002/nme.651)

A computational model for impact failure with shear-induced dilatancy

Z. Chen[1,*,†], R. Feng[2], X. Xin[1] and L. Shen[1]

[1]*Department of Civil and Environmental Engineering, University of Missouri-Columbia, Columbia, MO 65211-2200, U.S.A.*
[2]*Department of Engineering Mechanics, University of Nebraska-Lincoln, Lincoln, NE 68588-0526, U.S.A.*

SUMMARY

It has been observed in plate impact experiments that some brittle solids may undergo elastic deformation at the shock wave front, and fail catastrophically at a later time when they are shocked near but below the apparent Hugoniot elastic limit. Because this phenomenon appears to have features different from those of usual inelastic waves, it has been interpreted as the failure wave. To design an effective numerical procedure for simulating impact failure responses, a three-dimensional computational damage model is developed in this paper. The propagation of the failure wave behind the elastic shock wave is described by a non-linear diffusion equation. Macroscopic shear-induced dilatancy is assumed and treated as a one-to-one measure of the mean intensity of microcracking. The damage evolution in time is determined based on the assumption that the deviatoric strain energy in the elastically compressed material (undamaged) is converted, through the damaging process, into the volumetric potential energy in the comminuted and dilated material. For the ease in large-scale simulations, the coupled damage diffusion equation and the stress wave equation are solved via a staggered manner in a single computational domain. Numerical solutions by using both the finite element method and the material point method, i.e. with and without a rigid mesh connectivity, are presented and compared with the experimental data available. It is shown that the model simulations capture the essential features of the failure wave phenomenon observed in shock glasses, and that the numerical solutions for localized failure are not mesh-dependent. Copyright © 2003 John Wiley & Sons, Ltd.

KEY WORDS: failure wave; shear-induced dilatancy; damage diffusion; localization

1. INTRODUCTION

Under plate impact, some brittle solids may undergo elastic deformations at the shock wave front, and fail catastrophically at a distinctly later time if the shock stress is near but below

*Correspondence to: Z. Chen, Department of Civil and Environmental Engineering, University of Missouri-Columbia, E2509, Engineering Building East, Columbia, MO 65211-2200, U.S.A.
†E-mail: chenzh@missouri.edu

Contract/grant sponsor: AFOSR, ARO, NSF
Contract/grant sponsor: University of Nebraska-Lincoln

Received 17 August 2001
Revised 26 February 2002
Accepted 10 June 2002

the apparent Hugoniot elastic limit (HEL). The phenomenon has therefore been interpreted as the result of a slowly propagating failure wave in the shocked solids. Since Brar *et al.* [1] and Kanel *et al.* [2] reported the formation and propagation of failure waves in shocked glasses, continued efforts have been made to explore this interesting physical phenomenon, as shown by representative references [3–14]. However, no consensus can be made at the moment on the exact physics behind this failure wave phenomenon. Critical issues are what drives the failure wave, and how this physical phenomenon could be simulated in an effective way for large-scale simulation.

The shock response of glasses beyond the apparent HEL often displays a distinctive two-wave structure in wave profile. The trailing longitudinal stress wave is referred as the inelastic shock wave. However, in the shock wave experiments reported so far, no obvious jump in the longitudinal stress history has been detected at the failure wave front [1, 2, 7, 10]. One interpretation is that the apparent HEL may not be a true elastic limit, rather the manifestation of a transition in failure mechanisms. A possible transition is the one from a delayed kinetic-controlled failure process below the HEL to a prompt stress-controlled failure process above the HEL [8]. Another possibility is that the HEL may represent the stress level above which bulk glass undergoes permanent densification [10]. From existing experimental data available, however, the signature feature that separates the failure wave from the usual inelastic shock wave appears to be that only the lateral stress is changed significantly while the longitudinal stress history remains almost constant. In other words, the propagation of a 'failure wave' is not the result of momentum balance. The underlying mechanism must be a process governed by a field equation other than the stress wave equation.

It has been demonstrated that the jumps of certain kinematic variables in a complete failure process can be related to the transition between governing field equations of different types [15, 16]. By taking the initial point of material failure as one at which the change of governing equation type occurs (e.g. a hyperbolic type to an elliptic one for dynamic problems or one elliptic type to another for static problems), a moving material surface of discontinuity can be defined through the jump forms of conservation laws across the surface. Jumps in density, velocity, strain and stress can be determined on this moving surface of discontinuity between two material domains. Representing a hyperbolic-to-elliptic transition with a parabolic equation and using a linear local elastoplasticity model [17] and a non-linear local damage model [18], analytical solutions have been obtained for a dynamic softening bar and damaging bar, respectively. To obtain closed-form solutions, however, the speed of the moving surface of discontinuity was assumed to be constant, although a diffusing failure front may be resulted from the use of the jump forms of conservation laws [13]. Changes of governing equation type also arise in many thermal and fluid mechanics problems. For example, depending on the ratio of thermal diffusivity to relaxation time, heat may propagate at a finite speed as a thermal wave or at an infinite speed (in the absence of relaxation) as a thermal diffusion [19, 20]. Two different elliptic equations may hold respectively inside and outside of a turbulence domain [21].

From the available experimental, analytical and computational work on impact failure, it appears that the evolution of a failure wave resembles a process governed by the diffusion equation. Although the available information is not sufficient to identify the exact underlying physical mechanism, an attempt has been made to construct a micromechanics-based picture for the evolution of failure waves [14], based on the previous analytical and numerical study [13]. It has been proposed that under plane shock wave loading, the material failure below the

HEL occurs through simultaneous processes of heterogeneous microfissuring, shear dilatancy and void collapsing under high confining stresses, which result in an increase in the mean stress and a decrease in the deviatoric stress while all the longitudinal field variables remain unchanged. This particular form of failure initiates at the impact surface where the surface defects and transient loading conditions are conducive for such a process, and propagates into the material bulk through progressive multiplication of microfissures, thus a percolation process. As a result, the failure propagation is of diffusive nature. The physical mechanism proposed by Feng [14] is consistent with most of the available experimental observations on the failure wave phenomenon in shocked glasses. It also permits the use of a physically based field equation to describe the failure wave. However, the model is one-dimensional (1D) and difficult for implementation in general computer codes [14].

To design an effective numerical procedure for simulating impact failure responses, a three-dimensional (3D) computational damage model is developed in this paper, the model parameters of which can be calibrated based on the available experimental data. The propagation of the failure wave behind the elastic shock wave is described by a nonlinear diffusion equation. Macroscopic shear-induced dilatancy is assumed and treated as a one-to-one measure of the mean intensity of microcracking. The damage evolution in time is determined based on the assumption that the deviatoric strain energy in the elastically compressed material (undamaged) is converted, through the damaging process, into the volumetric potential energy in the comminuted and dilated material. To be efficient in large-scale simulation, the coupled damage diffusion equation and the stress wave equation are solved via a staggered manner in a single computational domain. Numerical solutions with the use of both the finite element method (FEM) and the material point method (MPM), i.e. with and without a rigid mesh connectivity, are presented and compared with experimental data available. Results of a parametric study are also presented to demonstrate the proposed procedure. It is shown that the model simulations capture the essential features of the failure wave phenomenon observed in shock glasses, and that the numerical solutions for localized failure are not mesh-dependent.

2. DAMAGE DIFFUSION

Higher order continuum models, such as nonlocal integral or strain gradient models, have been used to predict the evolution of localized failure, as reviewed by Chen and Schreyer [22]. However, the use of higher order models yields higher order governing differential equations with the ambiguity in the physics behind additional boundary conditions. On the other hand, discrete formulations such as decohesion and fracture-mechanics-based models as shown in representative references [23–25] introduce strong discontinuities into a continuum body such that the mathematical model is well-posed for given boundary and/or initial data. The discrete approaches could be promising if the bifurcation analysis is performed in an effective way to identify the onset and orientation of discontinuous failure modes based on the continuum tangent stiffness tensors. In this paper, a 3D damage diffusion equation is formulated to predict the evolution of microcracking in space without introducing any discontinuity. As a result, both damage diffusion and stress wave equations are classical in the sense that they are second order partial differential equations (PDE). The boundary conditions associated with each PDE can be identified based on the physics involved, and the numerical solutions are mesh-independent.

As indicated in the work by Feng [14] on the failure wave in shocked glasses, the surface imperfection and severe loading conditions at the impact surface may give rise to isolated microcracking in the vicinity of the impact surface. The formation of microcracks near the impact surface will in turn introduces local stress concentrations to the adjacent downstream material. Once these stress concentrations reach a certain threshold, microfissuring will be initiated there, and so on. Therefore, this process can be viewed as a progressive percolation of microfissures. It is macroscopically of diffusive nature, i.e. a diffusion process starting from a high concentration of microcracks to a low concentration of microcracks until a saturated state is reached in the 'continuum' or discontinuous failure occurs. Both microscopic heterogeneity and sufficient deviatoric strain energy are required to sustain such a diffusion process. If either the heterogeneity or deviatoric strain energy is not large enough, the diffusion process will not be active or die out eventually. From a viewpoint of energy conservation, the evolution of a failure wave in space converts the deviatoric strain energy in the intact material ahead of the failure front into the volumetric potential energy in the comminuted material behind the front. In other words, there will be a decrease in the stress deviator and an increase in the mean stress under the uniaxial strain conditions. For the plate impact problem considered here, both constitutive model and problem geometry are three-dimensional. Only due to the high confining pressure does the central part of the plate exhibit the uniaxial strain state during a very short time period in which the experimental data could be obtained.

The thermal effects are not considered here for simplicity. The problem of interest can then be formulated as an isotropic brittle continuum, which is subjected to an elastic shock compression governed by the usual nonlinear elastic wave equation, and experiences a delayed spatial evolution of damage governed by a diffusion equation. Since both the wave equation and diffusion equation are still the second order PDE, an effective numerical procedure can be developed with parallel computing for large-scale model-based simulation.

Since the wave equation is standard, it will not be discussed here. If the shear damage is assumed to induce material dilatancy, the average intensity of the material damage could be represented by an internal variable, the dilated volume, V_d. The dilated volume represents the increase in the specific volume of the material if it is damaged and then completely unloaded (in analogy to the definition of plastic strain). It should be pointed out that even if the shock wave compression is uniaxial, the percolation of microfissures occurs three-dimensionally. Therefore, a 3D diffusion equation in terms of V_d must be formulated to govern the evolution of damage in space. Note that the microscopic defects randomly distributed inside the material may initiate failure under shock compression, but will not result in the phenomenon of failure wave. Hence, for the purpose of this study, the bulk of the material is assumed to be flawless. The damage source is treated as an initial condition of V_d at the impact surface.

To describe the proposed governing equations and constitutive model, a direct notation is employed with boldfaced letters denoting tensors of first or higher order. The diffusion equation of V_d in the 3D space $\mathbf{x}$ with time t can be written as

$$\frac{\partial V_d}{\partial t} = \nabla \cdot [\mathbf{D}(\mathbf{x}, t) \cdot \nabla V_d] \tag{1}$$

where $\mathbf{D}(\mathbf{x}, t)$ denotes the second order damage diffusivity tensor. Owing to the lack of experimental data to calibrate an advanced constitutive model, a special case of isotropic damage is assumed here so that the model parameters can be calibrated and the result is consistent with the conversion of deviatoric potential energy into volumetric potential energy during the

failure evolution. Let $\mathbf{D}(\mathbf{x},t)=D(\mathbf{x},t)\mathbf{i}$ with $\mathbf{i}$ being the second order identity tensor and

$$D(\mathbf{x},t)=\begin{cases}0 & \text{if } Y\leqslant Y_{\mathrm{THD}} \text{ and } V_d=0\\ d\dfrac{Y-Y_{\mathrm{F}}}{Y_{\mathrm{HEL}}-Y_{\mathrm{F}}}\geqslant 0 & \text{if } Y>Y_{\mathrm{THD}} \text{ or } V_d>0\end{cases} \tag{2}$$

where d is the diffusion coefficient, Y is a proper variable representing the stress deviator in the material, e.g., the maximum shear stress or the second invariant of deviatoric stress, and subscripts 'F', 'HEL' and 'THD' denote the values of the stress deviator variable in the completely failed but compressed material, at the HEL, and at the threshold for initiating the failure process, respectively. As can be seen from Equation (2), the diffusion is inactive if the stress deviator variable is below Y_{THD}, and if the dilated volume is equal to zero. As long as $Y>Y_{\mathrm{THD}}$ or $V_d>0$, the diffusion process will be active until $Y=Y_{\mathrm{F}}$. Note that $Y<Y_{\mathrm{F}}$ during unloading.

Because most of the available experimental results on the failure wave phenomenon were reported as 'plane wave' measurements, it is difficult to uniquely determine the initial damage distribution (3D in general) from these data. It is clear, however, that the percolation of microdamage in a uniaxially shock-compressed material must be much faster in all the *lateral* (transverse) directions than in the longitudinal direction to result in a planar or nearly planar failure wave. Hence, it is reasonable to assume that the initial distribution of isolated microdamage sites near the impact surface is sufficiently uniform and planar. Thus, the evolution of failure in a uniaxially shock-compressed material can be considered as a pseudo-3D process, in which the initial damage distribution on the impact surface is assumed to be uniform and the propagation of failure is described by longitudinal diffusion supplemented with a time-dependent evolution function accounting for the much faster lateral percolation of microdamage at a given longitudinal location. In other words, for the case of failure wave under uniaxial shock compression, we may approximate Equations (1) and (2) using

$$\frac{\partial V_d}{\partial t}=\frac{\partial}{\partial x}\left[D(x,t)\frac{\partial V_d}{\partial x}\right]+Q(x,t) \tag{3a}$$

with

$$Q(x,t)=\frac{D(x,t)}{d}\frac{V_d-V_{d0}}{T_d}\geqslant 0 \tag{3b}$$

where $D(x,t)$ is a special case of Equation (2) considering only the variation in the longitudinal direction x, V_{d0} is the threshold below which $Q(x,t)$ is inactive, and T_d is the characteristic time for the lateral evolution of microdamage at a given longitudinal location. Although the partition between $D(x,t)$ and $Q(x,t)$ is not unique and a rigorous verification of the consistency between the effect of Equations (3) and that of Equations (1) and (2) remains a subject of further study, it is expected that the material parameters introduced here, namely, d, Y_{THD}, Y_{F}, V_{d0} and T_d, can be evaluated via well-defined impact experiments that measure the damage evolution profile and the residual frictional strength of comminuted material.

As can be seen from the above description, the propagation of the failure wave is simulated through the evolution of the internal state variable V_d in both temporal and spatial domains. If the material is shocked beyond the threshold Y_{THD} and an initial value of $V_d(>V_{d0})$ is assigned to the vicinity of the impact surface, a failure wave will propagate, behind the leading elastic

shock wave, through the material that is assumed to be initially flawless ($V_d = 0$). Note that although V_d increases during the damage diffusion, the specific volume of the compressed material, V, remains unchanged, and so do the macroscopic longitudinal stress and particle velocity.

3. CONSTITUTIVE MODELLING

The deformation kinematics and the 3D stress–strain relation that describe the response at a given material point are now considered. The key constitutive postulation is that the deviatoric potential energy in the intact material is converted into the volumetric potential energy in the comminuted and dilated material during the time-dependent failure evolution process. Hence, an increase of V_d results in a decrease of the deviatoric potential energy, which is reflected as an increase of lateral stresses. The Cauchy stress tensor and the strain tensors with respect to the deformed configuration are used in the description below.

The response of the shocked but intact material is assumed to be isotropic and non-linearly elastic. Following the convention used in shock wave analysis, the mean compressive stress in the intact material can be expressed as

$$\sigma_m = H(\mu) \tag{4a}$$

with

$$\mu = \frac{V_0}{V} - 1 \tag{4b}$$

where H is the Hugoniot mean stress function of the intact material, depending on the volume compression, μ, and V and V_0 denote the current and original specific volumes of the material, respectively. Once the failure process starts, however, the mean stress in the damaged material is assumed to depend on the average solid volume compression of the damaged material, μ_e but through the same functional relation, i.e.

$$\sigma_m = H(\mu_e) \tag{5a}$$

with

$$\mu_e = \mu + \frac{V_d}{V} = \frac{V_0 + V_d}{V} - 1 = \frac{\rho}{\rho_0} + \rho V_d - 1 \tag{5b}$$

in which ρ and ρ_0 represent the current and original mass densities, respectively. Note that Equations (4) are the special case of Equations (5) when $V_d = 0$. During the failure process, V_d and σ_m increase with damage at a fixed value of μ. In other words, there is no macroscopic volume change during the failure evolution, and the uniaxial-strain condition is preserved at the macroscopic level for the plate impact problem. Although Equations (5) represent a simple phenomenological approximation, it is expected to be useful as long as the damaged material is sufficiently compressed. Readers who are interested in further details of mean stress increase due to material dilatancy under large confining stresses are referred to the work by Curran *et al.* [26]. A useful and convenient approach is to express the Hugoniot mean stress response as a cubic function of μ_e, namely

$$\sigma_m = a_1\mu_e + a_2\mu_e^2 + a_3\mu_e^3 \tag{6}$$

where a_i are model parameters to be determined from experiments. The differential form of Equation (6) can be written as

$$\mathrm{d}\sigma_m = \frac{\partial \sigma_m}{\partial V}\,\mathrm{d}V + \frac{\partial \sigma_m}{\partial V_d}\,\mathrm{d}V_d \tag{7a}$$

with

$$\frac{\partial \sigma_m}{\partial V} = -(a_1 + 2a_2\mu_e + 3a_3\mu_e^2)\,\frac{V_0 + V_d}{V^2} \tag{7b}$$

and

$$\frac{\partial \sigma_m}{\partial V_d} = (a_1 + 2a_2\mu_e + 3a_3\mu_e^2)\,\frac{1}{V} \tag{7c}$$

Define the mean volumetric strain, ε_m as

$$3\varepsilon_m = \ln\frac{V}{V_0} = 3\varepsilon_m^e + 3\varepsilon_m^i \tag{8}$$

Assuming that the unloading of the *damaged* material from the compressed state (V) to the stress-free porous state ($V_0 + V_d$) is an elastic process, the elastic mean volumetric strain can be represented by

$$3\varepsilon_m^e = \ln\frac{V}{V_0 + V_d} \tag{9}$$

It then follows from Equations (8) and (9) that the inelastic mean volumetric strain is

$$3\varepsilon_m^i = \ln\frac{V_0 + V_d}{V_0} \tag{10}$$

which gives in a null ε_m^i when $V_d = 0$ as expected for consistency. It is evident from Equations (8)–(10) that the failure evolution does not change the current volume but, instead, changes the material state at full unloading.

The non-linear deviatoric response of the shocked intact material can be described by considering a pressure-dependent shear modulus, e.g.

$$G = b_0 + b_1\sigma_m + b_2\sigma_m^2 + b_3\sigma_m^3 \tag{11}$$

in which b_i are again model parameters to be determined from relevant experimental data. Let $\mathbf{s}$ and $\mathbf{e}$ denote the stress and strain tensors, and subscripts 'd' and 'v' the deviatoric and volumetric parts of these quantities, respectively. Then $\mathbf{s}_d = \mathbf{s} - \mathbf{s}_v$ and $\mathbf{e}_d = \mathbf{e} - \mathbf{e}_v$ with $\boldsymbol{s}_v = -\sigma_m\mathbf{i}$ and $\mathbf{e}_v = \varepsilon_m\mathbf{i}$. Hence, the differential deviatoric stress–strain relationship takes the form of

$$\mathrm{d}\mathbf{s}_d = 2G(\mathrm{d}\mathbf{e}_d - \mathrm{d}\mathbf{e}_d^{\mathrm{i}}) \tag{12}$$

where $\mathbf{e}_d^{\mathrm{i}}$ is the inelastic deviatoric strain due to damage. To calculate $\mathbf{e}_d^{\mathrm{i}}$, introduce a limit surface based on the energy conversion postulation described at the beginning of this section, namely

$$f = W_v^{\mathrm{e}} + W_d^{\mathrm{e}} - c = 0 \tag{13}$$

where W_v^e and W_d^e are the volumetric and deviatoric parts of elastic potential energy, respectively, and c represents the limit state at which failure occurs. The corresponding consistency condition can be written as

$$df = dW_v^e + dW_d^e = 0 \tag{14}$$

which requires

$$\mathbf{s}_v : d\mathbf{e}_v^e + \mathbf{s}_d : d\mathbf{e}_d^e = 0 \tag{15}$$

It is assumed that the failure wave behind the shock wave front will not cause additional strain at the macroscopic level under the plate impact conditions, as discussed before. This implies $d\mathbf{e}_v = d\mathbf{e}_d = 0$. Consequently, the relationships between the elastic and inelastic parts of volumetric and deviatoric strains have the form of

$$d\mathbf{e}_v^e = -d\mathbf{e}_v^i = -\frac{dV_d}{3(V_0 + V_d)}\mathbf{i} \tag{16a}$$

and

$$d\mathbf{e}_d^e = -d\mathbf{e}_d^i \tag{16b}$$

respectively. With the use of Equations (15) and (16), hence, it follows that

$$\frac{\sigma_m}{V_0 + V_d} dV_d - \mathbf{s}_d : d\mathbf{e}_d^i = 0 \tag{17}$$

Assuming $d\mathbf{e}_d^i = d\lambda \mathbf{s}_d$ in Equation (17) yields

$$d\lambda = \frac{\sigma_m}{(V_0 + V_d)\mathbf{s}_d : \mathbf{s}_d} dV_d > 0 \tag{18}$$

since $dV_d > 0$ with the evolution of failure. Thus, the differential inelastic deviatoric strain tensor takes the form of

$$d\mathbf{e}_d^i = \frac{\sigma_m \mathbf{s}_d}{(V_0 + V_d)\mathbf{s}_d : \mathbf{s}_d} dV_d \tag{19}$$

This completes the shear-dilatancy based, isotropic damage model needed for calculating the stress state in the material under the plate impact conditions. As can be seen from the above equations, the stress state depends on the value of V_d for the given strain state after material failure occurs behind the elastic shock wave.

To demonstrate the features of the proposed damage model, consider the incremental stresses during a failure evolution in a plate impact problem. The incremental longitudinal and lateral stresses are given by

$$\Delta s_{11} = (\Delta s_d)_{11} - \Delta\sigma_m \tag{20a}$$

and

$$\Delta s_{22} = \Delta s_{33} = (\Delta s_d)_{22} - \Delta\sigma_m \tag{20b}$$

respectively. Because the macroscopic strain field is unchanged in the failure zone behind the elastic shock wave, it follows from Equations (7), (12) and (19) that

$$\Delta s_{11} = -2G(\Delta e_d^i)_{11} - \frac{\partial \sigma_m}{\partial V_d}\Delta V_d$$
$$= -\frac{4G\sigma_m(s_{11}-s_{22})}{3(V_0+V_d)\mathbf{s}_d:\mathbf{s}_d}\Delta V_d - \frac{a_1+2a_2\mu_e+3a_3\mu_e^2}{V}\Delta V_d \tag{21a}$$

and

$$\Delta s_{22} = \Delta s_{33} = -2G(\Delta e_d^i)_{22} - \frac{\partial \sigma_m}{\partial V_d}\Delta V_d$$
$$= \frac{2G\sigma_m(s_{11}-s_{22})}{3(V_0+V_d)\mathbf{s}_d:\mathbf{s}_d}\Delta V_d - \frac{a_1+2a_2\mu_e+3a_3\mu_e^2}{V}\Delta V_d (<0 \text{ if } \Delta s_{11}=0) \tag{21b}$$

As can be seen from Equations (21), a suitable value of V_d may result in a zero change in the longitudinal stress but an increase in the absolute value of lateral stresses (note that $s_{11}<s_{22}=s_{33}<0$ in a plate impact problem).

4. NUMERICAL PROCEDURE

The numerical procedures for conventional wave and diffusion equations, with the use of the FEM or FDM, can be found in the standard books [27, 28]. For the coupled wave and diffusion problem considered in this paper, an accurate time integration procedure could be employed. However, the proposed constitutive model only simulates the essential feature of failure wave phenomena due to the lack of experimental data to calibrate a more advanced constitutive model. As a result, a simple computational procedure is designed here for the computational convenience in large-scale simulation, namely, central-difference in space and forward integration in time are used to solve the diffusion equation, while the FEM with constant stress elements in space and an explicit time integrator are employed to solve the wave equation with localized damage.

To simulate multi-physics shock responses of condensed matter, a robust spatial discretization procedure with flexible mesh connectivity is a necessity. Recently, several kinds of 'meshless' methods for spatial discretization have been proposed in the computational mechanics community. Since these meshless methods do not use a rigid mesh connectivity as compared with the conventional mesh-based methods such as FEM and FDM, they have been applied to some complex problems of current interests, as reviewed by Belytschko *et al.* [29]. Although academic exercises have demonstrated the robustness and potential of these meshless methods, they have not found their way successfully into general practical applications due to some unsolved problems such as moving surfaces of discontinuities, and the moving boundary conditions associated with the transition between different physical phenomena.

As one of the innovative spatial discretization methods, the material point method (MPM) is an extension to solid mechanics problems of a hydrodynamics code called FLIP which, in turn,

evolved from the particle-in-cell method. The motivation of the development was to simulate problems such as impact/contact, penetration and perforation with history-dependent internal state variables, as shown in the early publications about the MPM [30, 31]. The essential idea is to take advantages of both the Eulerian and Lagrangian methods while avoiding the shortcomings of each. Since the FEM and MPM represent the spatial discretization method with and without a rigid mesh connectivity, respectively, it is meaningful to verify the proposed staggered explicit time integration procedure for the coupled wave and diffusion problem by using both FEM and MPM. In addition, more confidence could be obtained before the MPM is applied to more complicated problems, if the FEM and MPM yield the similar solutions for the failure evolution without discontinuity.

To compare the numerical solutions via the FEM and those via the MPM, the updated Lagrangian formulation is used for the FEM. With the mapping from material points to the cell nodes of a background mesh and the mapping from the cell nodes to the material points in each time step, the MPM can be cast into the updated Lagrangian framework of the FEM [30, 31]. However, master/slave nodes are not needed in the MPM for impact problems due to the use of single-valued double mapping between material points and cell nodes. The matrix equations of displacement-based finite elements in the updated Lagrangian framework can be written as

$$[M]\{\ddot{u}\}^t = \{R\}^t - \{F\}_t^t + \{P\}_t^t \tag{22}$$

where $[M]$ is the time-independent diagonal mass matrix, $\{\ddot{u}\}^t$ the vector of nodal accelerations at time t, $\{R\}^t$ the vector of externally applied nodal loads at t, $\{F\}_t^t$ the vector of internal nodal forces at t measured with respect to the configuration at t, and $\{P\}_t^t$ the vector of artificial viscous damping forces at t measured with respect to the configuration at t. Thus, the velocity strain tensor can be obtained in each time step to find the corresponding Cauchy stress tensor through the constitutive model (details are described in the next paragraph). The internal nodal forces can then be calculated with respect to the current configuration. The inclusion of the artificial viscous damping forces with both a linear dependence term and a quadratic one on the nodal acceleration is to eliminate the numerical oscillation (Gibbs' phenomenon) behind the shock wave front. The critical time step for stable integrations of both the wave and diffusion equations is calculated for each cycle to determine a proper time step for the following cycle and so on. Although the wave and diffusion equations are coupled through the internal variable V_d after failure occurs, a simple procedure is adopted in this work. That is to solve the wave and diffusion equations in a parallel (staggered) setting. For the target and flyer involved in the plate impact, plane strain rectangles (each consisting of four triangular elements) are used in the FEM, while four material points in each plane cell are employed in the MPM.

With the use of explicit time integration, the implementation of the damage model into the FEM and MPM codes is straightforward. For each time increment, Δt, diffusion calculation gives ΔV_d. To determine the corresponding stress state, compute sequentially:

1. $\mu_e = \dfrac{V_0 + V_d|^t}{V|^t} - 1$ with $V_d|^t = V_d|^{t-\Delta t} + \Delta V_d$;
2. $\sigma_m = a_1\mu_e + a_2\mu_e^2 + a_3\mu_e^3$;
3. $G = b_0 + b_1\sigma_m + b_2\sigma_m^2 + b_3\sigma_m^3$;

4. $\Delta \mathbf{e}_d^{\mathrm{i}} = \dfrac{\sigma_m \mathbf{s}_d}{(V_0 + V_d|^t)\mathbf{s}_d : \mathbf{s}_d} \Delta V_d$;
5. $\Delta \mathbf{s}_d = 2G(\Delta \mathbf{e}_d - \Delta \mathbf{e}_d^i)$ with $\Delta \mathbf{e}_d = \Delta \mathbf{e} - \Delta \mathbf{e}_v$ and $\Delta \mathbf{e}_v = \mathbf{e}_v|^t - \mathbf{e}_v|^{t-\Delta t}$; and
6. $\mathbf{s}|^t = \mathbf{s}|^{t-\Delta t} + \Delta \mathbf{s}$ with $\Delta \mathbf{s} = \Delta \mathbf{s}_d + (-\Delta \sigma_m)\mathbf{i}$ and $\Delta \sigma_m = \sigma_m|^t - \sigma_m|^{t-\Delta t}$.

5. DEMONSTRATION

Although the failure wave phenomenon has been observed in several glasses, a complete set of data that permit the determination of the material parameters describing both the elastic shock response and the failure wave phenomenon in a given material is not currently available in the literature. To demonstrate the proposed model and to validate the numerical procedure, the method used by Feng [14] will be adopted here. That is to describe the elastic shock wave response of the model material as that of soda lime glass whose shock response has been well characterized, [8, 14, 32] and to model its failure evolution characteristics as that of K-8 glass for which the lateral stress history during the failure process has been reported by Kanel *et al*. [2]. Both the numerical results and experimental data are normalized appropriately to construct a meaningful comparison.

Specifically, the original mass density, longitudinal and shear sound speeds, and apparent HEL stress of the model material are $\rho_0 = 2530$ kg/m^3, $c_L = 5828$ m/s, $c_S = 3468$ m/s and $\sigma_{\mathrm{HEL}} = 5.95$ Gpa, respectively, using the results from the work by Holmquist *et al*. [32] on a soda lime glass. Furthermore, fitting their mean stress results with Equation (6) gives, in unit of GPa

$$\sigma_m = 45.36\mu_e - 137.0\mu_e^2 + 288.3\mu_e^3 \tag{23}$$

Based on the longitudinal stress response obtained from a Lagrangian analysis of the shock wave profiles obtained in the same glass [8] and Equation (23), the shear modulus [Equation (11)] can be quantified as

$$G = 30.43 + 1.485\sigma_m - 0.6009\sigma_m^2 - 0.3479\sigma_m^3 \tag{24}$$

again in unit of GPa. Using $Y = |s_{11} - s_{22}|$ as the stress deviator measure leads to the following material parameters: $Y_{\mathrm{HEL}} = 4.529$ Gpa and $Y_{\mathrm{THD}} = 2.243$ Gpa (which corresponds to a threshold shock stress of 3 Gpa). It is further assumed that the failure process would result in a 50% increase in the lateral stress, at which $Y = Y_{\mathrm{F}}$ and $D(x,t) = 0$ in Equations (2), in accordance with the experimental data on a K-8 glass [2].

A series of numerical calculations based on the above material model have been carried out to determine the material parameters d, T_d and V_{d0} that provide the best simulation of the failure evolution characteristics observed in the shocked K-8 glass. The results of one of the calculations are presented in Figure 1 in terms of a comparison between the computed and measured lateral stress histories, each normalized with respect to the respective lateral stress before the failure wave front for the reason discussed in the beginning paragraph of this section. For clarity, a sound speed of 5828 m/s was used to correlate the profiles at 4.5 mm (from the impact surface) and those at 6.5 mm. The damage diffusion parameters used in this calculation were: $d = 12$ m^2/s, $T_d = 7.7 \times 10^{-9}$ s and $V_{d0} = 5.0 \times 10^{-7}$ m^3/kg. As shown in Figure 1, the model calculation simulates the essential features in the experimental data

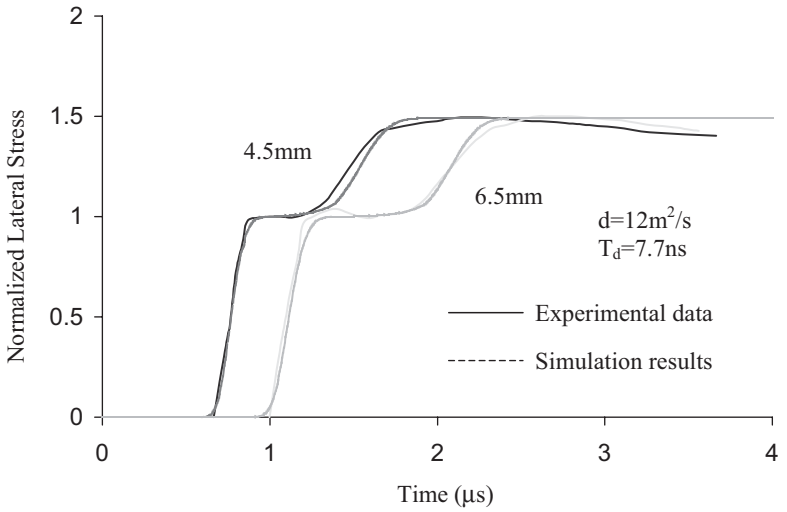

Figure 1. Comparison of the model prediction with experimental data.

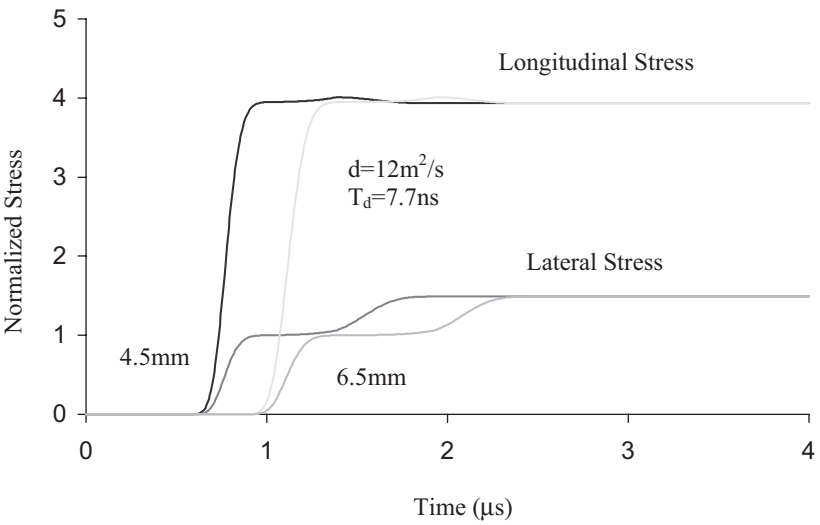

Figure 2. The longitudinal and lateral stresses of model prediction corresponding to Figure 1.

very well. The corresponding longitudinal stress histories at the two locations are shown in Figure 2. As can be seen, there is no significant change in the longitudinal stress during the failure evolution. The very small variation during the initial acceleration of damage evolution is due to numerical inaccuracy since no iteration is used in the evaluation of $\Delta \mathbf{e}_d^i$ for simplicity. As expected, however, the small variation dies out quickly as the failure evolution slows down towards the equilibrium state.

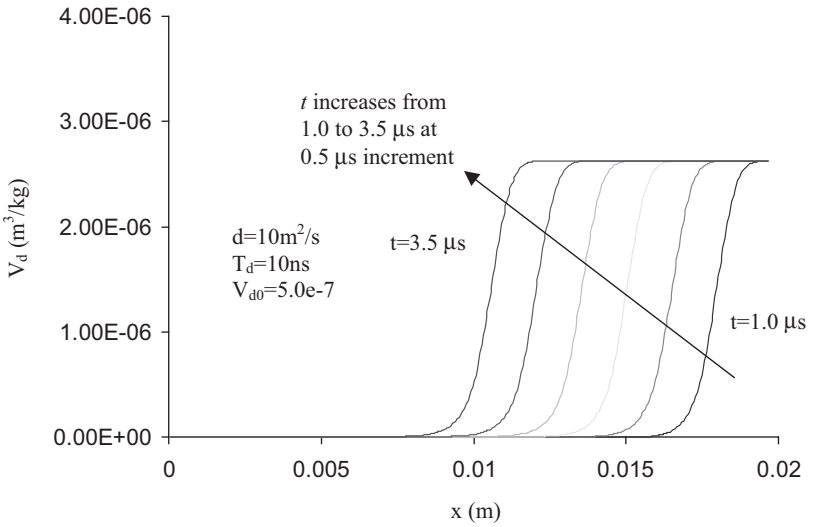

Figure 3. The profiles of V_d at different times.

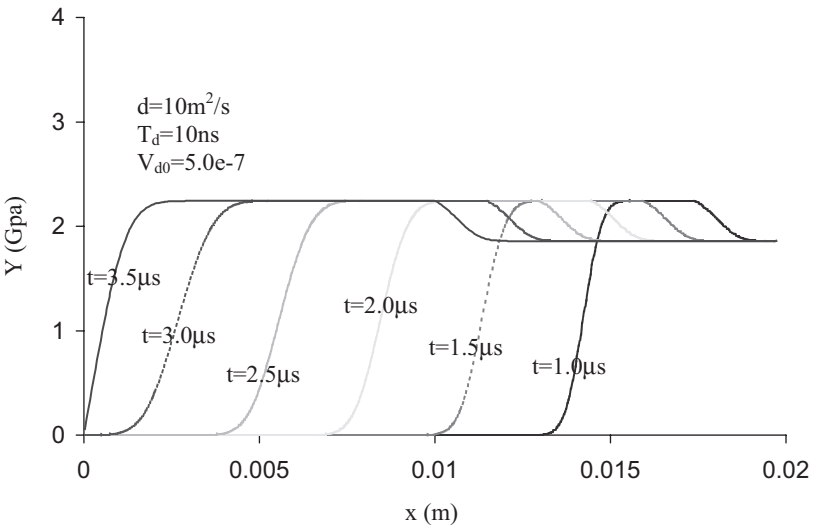

Figure 4. The profiles of Y corresponding to Figure 3.

A series of snap shots of the distributions of V_d (macroscopic measure of damage) in the interior of the target are presented in Figure 3 for times from 1.0 to 3.5 μs after the impact occurs at $x = 0.02$ m. The results demonstrate clearly the failure evolution governed by Equations (3). The snap shots of the corresponding distributions of the stress deviator measure ($Y = |s_{11} - s_{22}|$) are shown in Figure 4. As can be seen in each profile, Y increases to the peak with the passage of elastic shock wave, and decreases to a lower value due to the evolution of failure. The separation between the elastic shock wave and failure fronts increases with

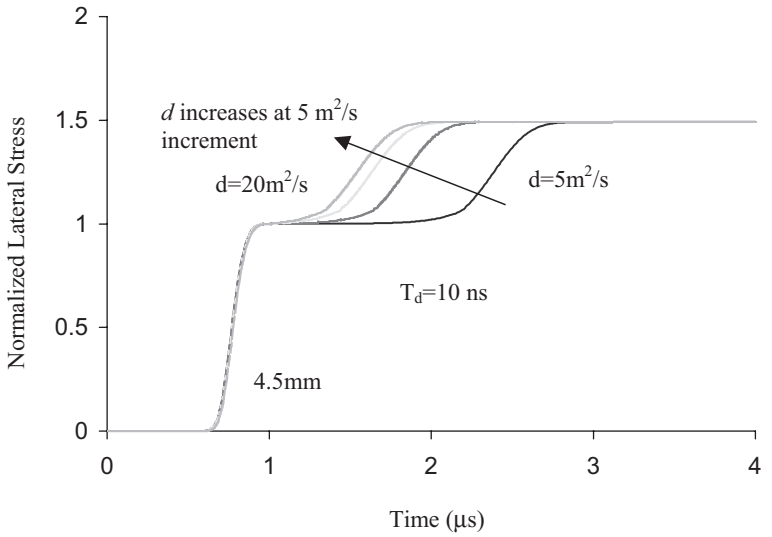

Figure 5. Effect of damage diffusivity.

the distance from the impact. This is the characteristic feature that separates the failure wave phenomenon from the usual time-dependent material response.

To further demonstrate the proposed procedure, a parametric study has been conducted to examine how the failure evolution characteristics are influenced by the damage diffusion coefficient, d and the characteristic time for lateral evolution of damage, T_d. The results presented in Figure 5 are from four calculations with increasing values of d from 5 to $20\,\mathrm{m}^2/\mathrm{s}$ at an increment of $5\,\mathrm{m}^2/\mathrm{s}$. The value of T_d (10 ns) was kept unchanged and so were the values of the other model parameters. The numerical results indicated that though non-proportional the propagation speed of the failure wave increases with d. The shape of the failure evolution from its onset to completion, however, remains unchanged.

The examination for the effects of T_d is given in Figure 6. The value of T_d was decreased in four steps from 20 to 1 ns while $d(10\,\mathrm{m}^2/\mathrm{s})$ was held unchanged along with the other parameters. Unlike the effects of varying d, a smaller T_d results in not only a faster propagation of failure in the longitudinal direction but also a faster lateral percolation of damage as indicated by a steeper rise in the lateral stress evolution associated with failure process. In fact, as can be seen in Figure 6, if T_d is small enough (i.e. the lateral percolation of damage is fast enough) the two steps in the lateral stress profile may merge into one. When this happens, the process can also be described as a single inelastic shock wave.

The convergence study is performed with three meshes for both stress histories and profiles, as shown in Figures 7 and 8, respectively. As can be seen, the numerical solutions converge very fast.

To compare the FEM with the MPM, the MPM solutions corresponding to Figures 1 and 2 are presented in Figures 9 and 10, and those corresponding to Figures 7 and 8 are shown in Figures 11 and 12. As can be observed from these figures, the wave fronts in the MPM solutions look sharper than those in the FEM solutions, while both the FEM and MPM yield the similar solutions features.

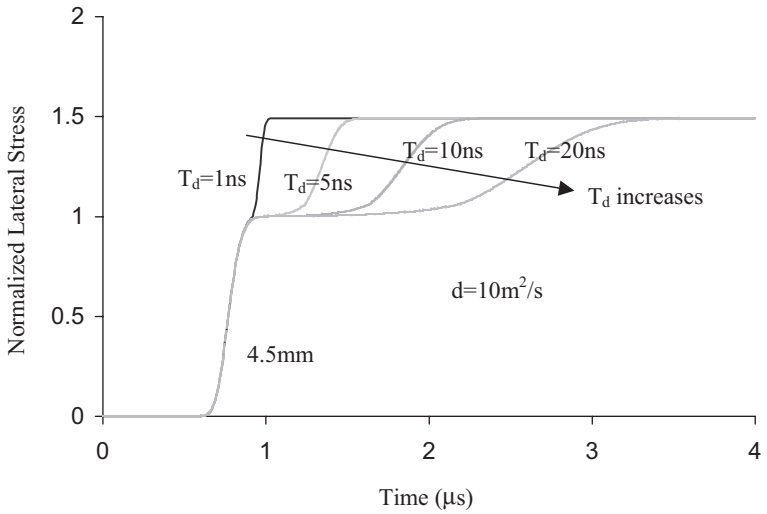

Figure 6. Effect of the characteristic time of damage evolution.

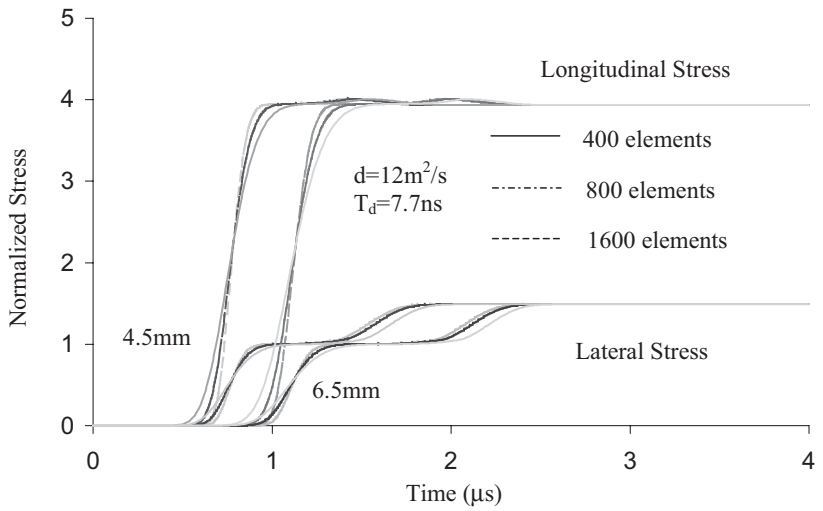

Figure 7. The convergence of the longitudinal and lateral stress histories by using the FEM.

6. CONCLUDING REMARKS AND FUTURE RESEARCH

To design an effective numerical procedure for simulating large-scale impact failure responses, a three-dimensional computational damage model has been developed in this paper. The propagation of the failure wave behind the elastic shock wave is described by a non-linear diffusion equation. Macroscopic shear-induced dilatancy is assumed and treated as a one-to-one measure of the mean intensity of microcracking. The damage evolution in time is determined based

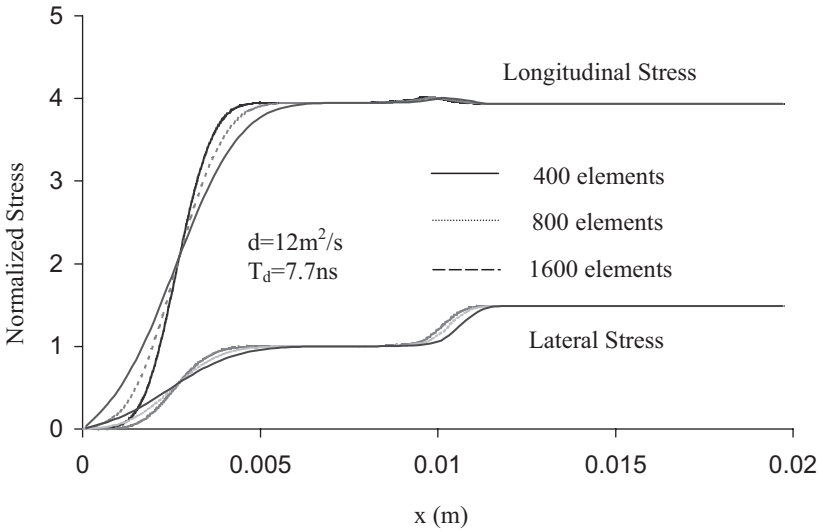

Figure 8. The convergence of the stress profiles at $t = 3.0$ μs by using the FEM.

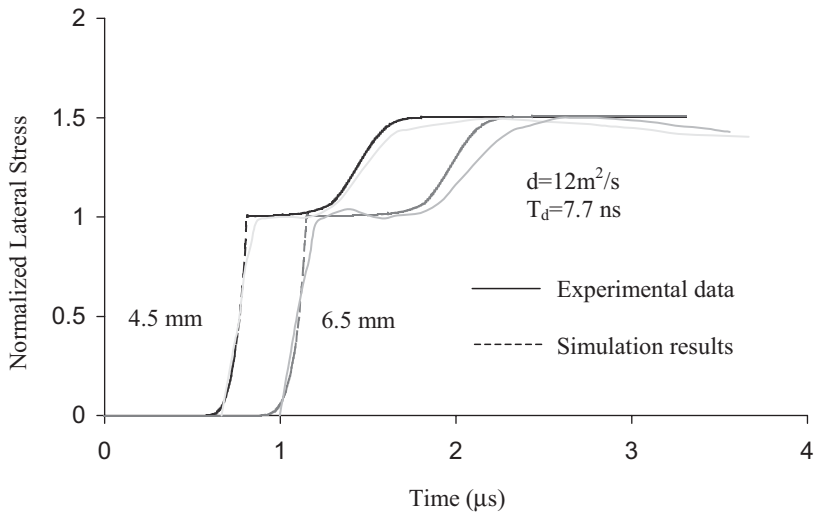

Figure 9. Comparison of the model prediction with experimental data by using the MPM.

on the assumption that the deviatoric strain energy in the elastically compressed material is converted, through the damaging process, into the volumetric potential energy in the comminuted and dilated material. The damage diffusion equation and the stress wave equation are solved via a staggered manner in a single computational domain. Numerical solutions by using both the FEM and the MPM are presented and compared with experimental data available. It is shown that the model simulations capture the essential features of the failure

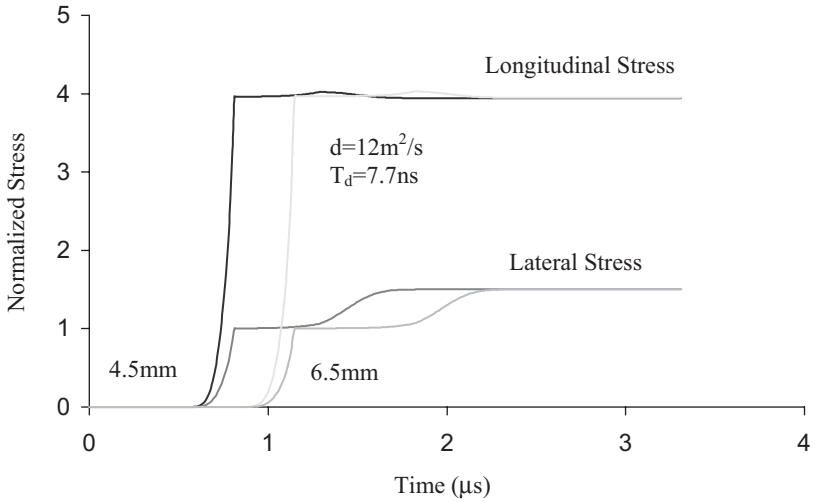

Figure 10. The longitudinal and lateral stresses of model prediction corresponding to Figure 9.

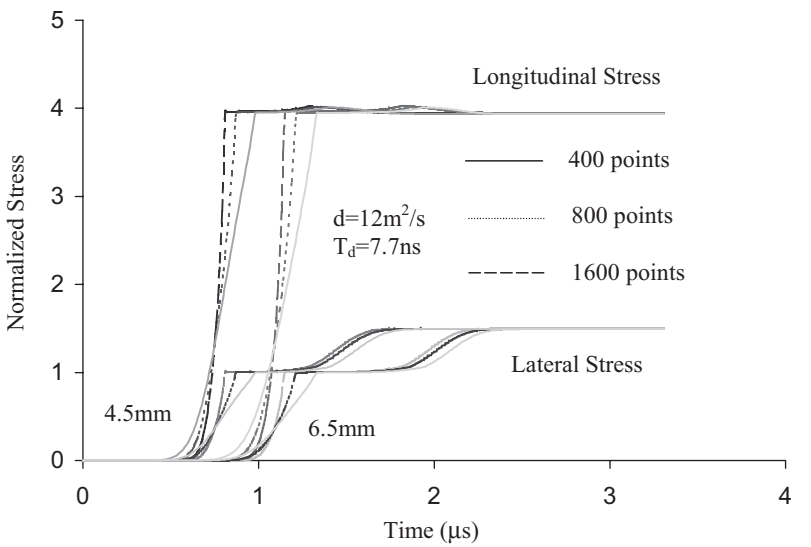

Figure 11. The convergence of the longitudinal and lateral stress histories by using the MPM.

wave phenomenon observed in shock glasses, and that the numerical solutions for localized failure converge very fast.

However, the model validation is limited to a uniaxial-strain problem due to the lack of systematic experimental data. Well-defined experiments, particularly those providing measurements for 3D diffusion of damage are needed to validate the model and solution procedures more rigorously. An integrated experimental, analytical and computational effort is necessary

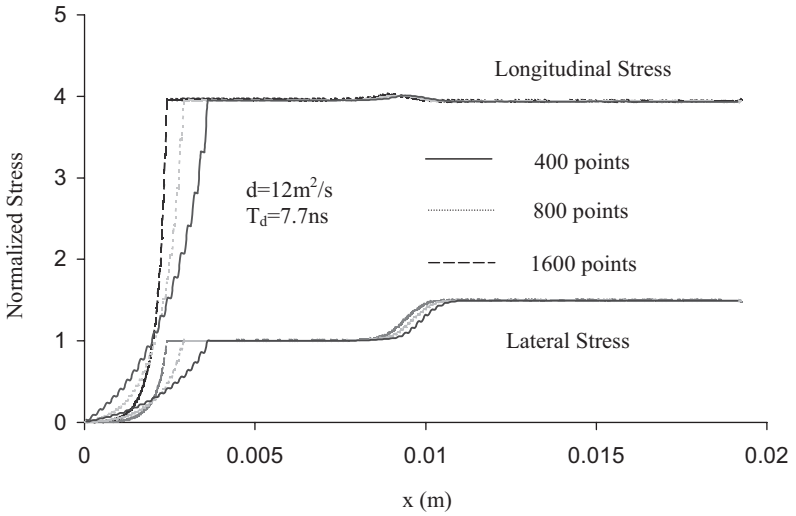

Figure 12. The convergence of the stress profiles at $t = 3.0\,\mu s$ by using the MPM.

to develop a better understanding of the formation and propagation of failure in brittle solids subjected to impulsive loading.

ACKNOWLEDGEMENTS

This work was sponsored (in part) by AFOSR, ARO and NSF. One of the authors (RF) gratefully acknowledges the support by the University of Nebraska-Lincoln through a Faculty Fellowship. The authors are also grateful to Prof. Kanel and Dr Razorenov at the Institute of Problems of Chemical Physics of the Russian Academy of Sciences, for valuable joint discussion on the failure wave phenomenon when they recently visited the University of Missouri-Columbia. The authors are also grateful to the reviewers for discerning comments on this paper.

REFERENCES

1. Brar NS, Bless SJ, Rosenberg Z. Impact-induced failure waves in glass bars and plates. *Applied Physics Letters* 1991; **59**:3396–3398.
2. Kanel GI, Rasorenov SV, Fortov VE, 1992. The failure waves and spallations in homogeneous brittle materials. In *Shock Compression of Condensed Matter—1991*, Schmidt SC, Dick RD, Forbes JW, Tasker DG (eds). Elsevier: New York, 1992; pp. 451–454.
3. Clifton RJ. 1993. Analysis of failure waves in glasses. *Applied Mechanics Reviews* (ASME) 1993; **46**: 540–546.
4. Bless SJ, Brar NS. Impact induced fracture of glass bars. In *High-Pressure Science and Technology*, Schmidt SC, Shaner JW, Samana GA, Ross M (eds). AIP: New York, NY, 1994; 1813–1816.
5. Raiser G, Clifton RJ. Failure waves in uniaxial compression of an aluminosilicate glass. In *High-Pressure Science and Technology*, Schmidt SC, Shaner JW, Samana GA, Ross M (eds). AIP: New York, 1994; 1039–1042.
6. Raiser GF, Wise JL, Clifton RJ, Grady DE, Cox DE. Plate impact response of ceramics and glasses. *Journal of Applied Physics* 1994; **75**:3862–3869.
7. Bourne NK, Rosenberg Z, Field JE. High-speed photography of compressive failure waves in glasses. *Journal of Applied Physics* 1995; **78**:3736–3739.
8. Grady DE. 1996. Shock-wave properties of brittle solids. In *Shock Compression of Condensed Matter—1995*, Schmidt SC, Tao WC (eds). AIP: New York, 1996; 9–20.

9. Rosenberg Z, Bourne NK, Millett JCF. Direct measurements of strain in shock-loaded glass specimens. *Journal of Applied Physics* 1996; **79**:3971–3974.
10. Espinosa HD, Xu Y, Brar NS. Micromechanics of failure waves in glass: experiments. *Journal of the American Ceramic Society* 1997a; **80**:2061–2073.
11. Espinosa HD, Xu Y, Brar NS. Micromechanics of failure waves in glass: modeling. *Journal of the American Ceramic Society* 1997b; **80**:2074–2085.
12. Partom Y. Modeling failure waves in glass. *International Journal of Impact Engineering* 1998; **21**:791–799.
13. Chen Z, Xin X. An analytical and numerical study of failure waves. *International Journal of Solids and Structures* 1999; **36**:3977–3991.
14. Feng R. Formation and propagation of failure in shocked glasses. *Journal of Applied Physics* 2000; **87**: 1693–1700.
15. Chen Z, Sulsky D. A partitioned-modeling approach with moving jump conditions for localization. *International Journal of Solids and Structures* 1995; **32**:1893–1905.
16. Chen Z. Continuous and discontinuous failure modes. *Journal of Engineering Mechanics* (ASCE) 1996; **122**: 80–82.
17. Xin X, Chen Z. An analytical solution with local elastoplastic models for the evolution of dynamic softening. *International Journal of Solids and Structures* 2000; **37**:5855–5872.
18. Xin X, Chicone C, Chen Z. Analytical solutions for failure evolution with a nonlinear local damage model. *Journal of Applied Mechanics* (ASME) 2001; **68**:835–843.
19. Tzou DY. On the thermal shock wave induced by a moving heat source. *Journal of Heat Transfer* (ASME) 1989; **111**:232–238.
20. Tzou DY. *Macro- to Microscale Heat Transfer: The Lagging Behavior*. Taylor & Francis: Washington, DC, 1997.
21. Chen Z, Clark T. Some remarks on domain-transition problems. *Archives of Mechanics* 1995; **47**:499–512.
22. Chen Z, Schreyer HL. On nonlocal damage models for interface problems. *International Journal of Solids and Structures* 1994; **31**:1241–1261.
23. Xu XP, Needleman A. Numerical simulations of dynamic crack growth along an interface. *International Journal of Fracture* 1996; **74**:289–324.
24. Oritz M, Pandolfi A. Finite-deformation irreversible cohesive elements for three-dimensional crack-propagation analysis. *International Journal for Numerical Methods in Engineering* 1999; **44**:1267–1282.
25. Schreyer HL, Peffer A. Fiber pullout based on a one-dimensional model of decohesion. *Mechanics of Materials* 2000; **32**:821–836.
26. Curran DR, Seaman L, Cooper T, Shockey DA. Micromechanical model for comminution and granular flow of brittle material under high strain rate application to penetration of ceramic targets. *International Journal of Impact Engineering*, 1993; **13**:53–83.
27. Belytschko T, Hughes T (eds). *Computational Methods for Transient Analysis* 1. Elsevier: Amsterdam, 1983.
28. Reddy JN, Gartling DK. *The Finite Element Method in Heat Transfer and Fluid Dynamics*. CRC Press: Boca Raton, FL, 1994.
29. Belytschko T, Krongauz Y, Organ D, Fleming M, Krysl P. Meshless methods: an overview and recent developments. *Computer Methods in Applied Mechanics and Engineering* 1996; **139**:3–48.
30. Sulsky D, Chen Z, Schreyer HL. A particle method for history-dependent materials. *Computer Methods in Applied Mechanics and Engineering* 1994; **118**:179–196.
31. Sulsky D, Zhou SJ, Schreyer HL. Application of a particle-in-cell method to solid mechanics. *Computer Physics Communications* 1995; **87**:236–252.
32. Holmquist TJ, Johnson GR, Grady DE, Lopatin CM, Herfel ES. High strain rate properties and constitutive modeling of glass. *15th International Symposium on Ballistics*, Jerusalem, Israel, 1995; 237–244.

